Magneto-hydrodynamics of couple stress lubricants in combined squeeze and shear in parallel annular disc viscous coupling systems

M. Daliri[1], D. Jalali-Vahid[1] and H. Rahnejat[2]

[1] Sahand University of Technology, Tabriz, Iran

[2]Wolfson School of Mechanical and Manufacturing Engineering,

Loughborough University, UK

Abstract:

This paper presents predictive analysis of load carrying capacity, tractive efficiency and response time of parallel annular discs intervened with a film of lubricant under combined shear and squeeze film motions. This configuration represents operational characteristics of viscous coupling systems. In particular, the case of viscous dampers for tractive torque generation and distribution in all-wheel-drive off-road vehicles is studied. Various forms of lubricant behaviour, from idealised Newtonian to that of non-Newtonian silicone-based fluids and incompressible isothermal electrically conducting couple stress fluids, subjected to a magnetic field are studied (MHD). The solution for the MHD includes combined solution of modified Reynolds equation and Stoke's micro-continuum for couple stress fluids in squeeze and shear with rotational fluid inertia, an approach not hitherto reported in literature.

It is shown that in general MHD couple stress fluids enhance the load carrying capacity of the contact and inhibit the incidence of thin films which can result in direct contact of surfaces. Rotational inertia decreases the load carrying capacity, although in general the MHD fluids show better load carrying capacity and tractive efficiency than the other alternatives. However, they exhibit a lower response time under the assumed isothermal condition. Nevertheless, the MHD fluids are best suited to applications in viscous coupling systems because of their controllability.

Keywords: Couple stress fluids, Hartman number, parallel annular discs, Stokes micro-continuum theory, rotational inertial effects, viscous coupling systems, All-wheel-drive vehicles.

1. Introduction

Increasingly higher loads are carried by lubricated conjunctions in many machines and mechanisms such as in vehicular drive trains at high lubricant shear rates. These conditions often result in very thin films operating at limiting shear stress of the lubricant [1]. One repercussion can be direct interaction of surfaces. Furthermore, contact conjunctions are also expected to operate with ever decreasing frictional losses in order to improve energy efficiency, particularly in vehicles which need to meet stringent emission criteria such as compliance with the new

European drive cycle [2]. Additionally, the drive for improved fuel efficiency has brought about technologies such as cylinder deactivation (CDA) which improve upon fuel efficiency, but often at the expense of noise, vibration and harshness (NVH) refinement, which is another growing area of concern in the competitive automotive sector. A result of application of CDA is exacerbated engine order vibration which can transmit larger oscillatory motions to drive train components [3]. Therefore, palliative measures are required to reduce the untoward effects of impulsive actions with application of new technologies such as hybridization, cylinder deactivation and the increasing tendency in high output power to weight ratio compact engines.

One approach is the use of viscous dampers, such as visco-lock systems with high load carrying capacity and with a lubricant of suitable thixotropic non-Newtonian shear characteristics such as silicone-based lubricants, which transmit torque through good traction. Sharaf et al [4] include a rheological model for silicone-based lubricants in visco-lock devices used in off-road all-wheel-(AWD) vehicles, subjected to various tractive motions on different terrains.

Another approach is the growing trend in the use of electrically conducting fluids in some machines and mechanisms. The aim is to avoid the undesired and unpredictable changes in the viscosity of lubricant with temperature and/or pressure. Thus, use of electro-rheological (ERF) lubricants, magneto- rheological fluids (MRF) and nano-fluids have been receiving increasing attention.

A number of empirical and theoretical studies have investigated the performance characteristics of magneto-hydrodynamic (MHD) thin film bearings with different contact geometries in the presence of generated external magnetic fields. Some representative experimental and numerical studies include the MHD squeeze film characteristics by Maki and Kuzma[5], Usha and Vimala [6], Lin et al. [7], Lin [8] and Hsu et al [9]. Additionally, Agrawal [10], Anwar and Rodkiewich [11], and Gupta and Bhat [12] have studied the lubricant behaviour in MHD slider bearings.

The rheological flow behaviour of a Newtonian lubricant, blended with various additives cannot be accurately described by the classical continuum theory. Therefore, many micro-continuum theories have been proposed [13-18], involving the use of the couple stress concept, which was originally developed to model non-Newtonian fluids such as synthetic fluids, polymer-thickened oils, liquid crystals, and even blood. In this method the sizes of blended particles are important. However, the couple stress concept in micro-contiuum theory is a simplified version of the higher order/higher-grade micropolar continuum theory [19,20], where rotational degrees of freedom of particles are also taken into account in addition to their translational degrees of freedom in shear. Therefore, the size effects at small scale are not properly represented in the couple stress approach. However, the computational effort is significantly reduced and analytical formulation becomes possible. As a result, this simplified approach has led to the study of various conjunctions such as squeeze film lubrication in thrust bearings by Ramanaish and Sarkar [21] and Das [22] for the lubrication of slider bearings with an MHD couple stress fluid as the lubricant and in the presence of an external magnetic field.

Recently, Daliri et al [23] studied the combined effects of MHD coupled stress lubricant, including the effect of convective inertia between wide parallel rectangular plates. In order to address practical applications of the theory, in this paper the geometry of wide parallel rectangular plates is altered to represent parallel annular discs under combined squeeze and rotation to represent visco-lock systems described by Sharaf et al [4]. Therefore, the current study is divided into two parts. First, the characteristics of squeeze film lubrication between rotating parallel annular discs is undertaken. Then, the application of MHD coupled stress lubricant to annular discs in rotation for visco-lock vehicular differentials is considered.

The results of squeeze film characteristics such as the load- carrying capacity and time history of film thickness are presented for various values of coupled stress parameter, radius ratio, lubricant rotational inertia and the Hartman's number. An important consideration is the generated tractive torque for various values of coupled stress parameter, outer and inner plate radii and the operating differential speed between the inner and outer plates as well as the Hartman's number.

2. The analytical approach

2.1- characteristics of squeeze film:

The geometry of the problem between two parallel annular discs with inner radius *b* and outer radius *a* is shown in figure 1, in which the upper disc rotates at an angular velocity Ω and approaches the lower disc with a constant squeezing velocity *V*. It is necessary to calculate the pressure distribution, load carrying capacity and film thickness. The momentum equations for a MHD coupled stress fluid are used in the presence of a uniform magnetic field, including the rotational fluid inertia. Therefore, the governing equations are obtained as follows:
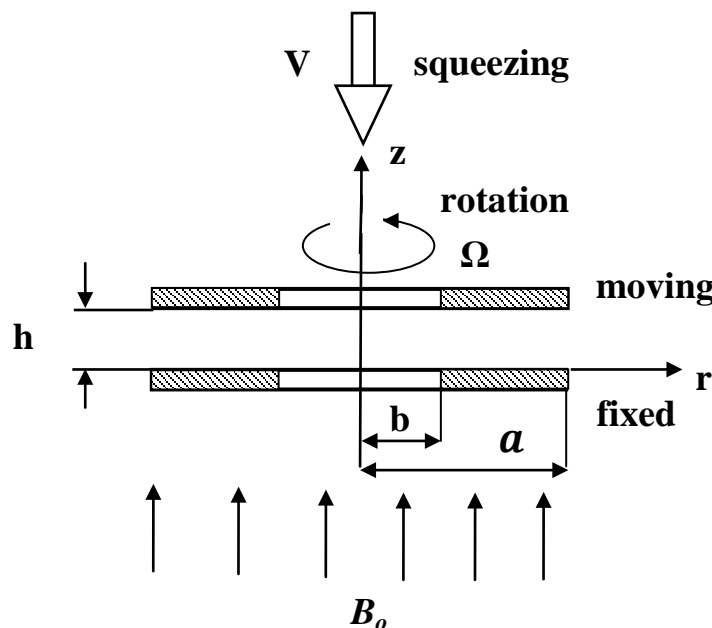

Fig1. Squeeze film geometry between two parallel annular discs

$$-\rho \frac{v^2}{r} = -\frac{\partial p}{\partial r} + \mu \frac{\partial^2 u}{\partial z^2} - \eta \frac{\partial^4 u}{\partial z^4} - \sigma B_o^2 u \tag{1}$$

$$0 = \mu \frac{\partial^2 v}{\partial z^2} - \eta \frac{\partial^4 v}{\partial z^4} - \sigma B_o^2 v \tag{2}$$

$$\frac{\partial p}{\partial z} = 0 \tag{3}$$

The derivation of equations (1)-(3) with the underlying assumptions made is provided in Appendix 2.

The continuity equation is:

$$\frac{1}{r} \frac{\partial (r u)}{\partial r} + \frac{\partial w}{\partial z} = 0 \tag{4}$$

where u, v and w are velocity components in the r, θ and z directions respectively. η is the material constant for the couple stress fluid, σ is the electrical conductivity of the lubricant and B_o represents the applied magnetic field.

The boundary conditions in the lubricant region and with no- couple stress conditions [13] at surfaces are:

$$u = 0, \quad \frac{\partial^2 u}{\partial z^2} = 0, w = 0 \quad at \; z = 0 \tag{5}$$

$$u = 0 \;, \quad \frac{\partial^2 u}{\partial z^2} = 0, w = \frac{dh}{dt} \quad at \; z = h \tag{6}$$

$$v = 0, \quad \frac{\partial^2 v}{\partial z^2} = 0 \quad at \; z = 0 \tag{7}$$

$$v = r\Omega, \quad \frac{\partial^2 v}{\partial z^2} = 0 \quad at \; z = h \tag{8}$$

The boundary conditions for the film pressure p are given as:

$$p(b) = 0 \tag{9}$$

$$p(a) = 0 \tag{10}$$

4

Making use of non-dimensional parameters:

$$l = (\frac{\eta}{\mu})^{\frac{1}{2}}, l^* = \frac{l}{h_o}, a^* = \frac{1}{l^*}, z^* = \frac{z}{h_o}, h^* = \frac{h}{h_o}, M = B_o h_o \sqrt{\frac{\sigma}{\mu}}, v^* = \frac{v}{r\Omega} \tag{11}$$

the dimensionless form of equation (2) becomes:

$$\frac{\partial^4 v^*}{\partial z^{*4}} - a^{*2} \frac{\partial^2 v^*}{\partial z^{*2}} + M^2 a^{*2} v = 0 \tag{12}$$

The non-dimensional forms of boundary conditions (7, 8) are:

$$v^* = 0, \quad \frac{\partial^2 v^*}{\partial z^{*2}} = 0 \quad at \ z^* = 0 \tag{13}$$

$$v^* = 1, \quad \frac{\partial^2 v^*}{\partial z^{*2}} = 0 \quad at \ z^* = h^* \tag{14}$$

Noting that: $\frac{\partial p}{\partial r} - \frac{\rho}{r} v^2 = g_p$ and $u^* = \frac{\mu u}{h_o^2(-g_p)}$, equation (1) is transformed to:

$$\frac{\partial^4 u^*}{\partial z^{*4}} - a^{*2} \frac{\partial^2 u^*}{\partial z^{*2}} + M^2 a^{*2} u^* = a^{*2} \tag{15}$$

The non-dimensional form of boundary conditions (5,6) are:

$$u^* = 0 \ , \quad \frac{\partial^2 u^*}{\partial z^{*2}} = 0 \quad at \ z^* = 0 \tag{16}$$

$$u^* = 0 \ , \quad \frac{\partial^2 u^*}{\partial z^{*2}} = 0 \quad at \ z^* = h^* \tag{17}$$

The boundary conditions (13) and (14) are used for the solution of equation (12) and the boundary conditions (16) and (17) are used for the solution of equation (15). This yields the velocity distribution across the lubricant film in θ and r directions respectively. Three different cases are considered according to the parameter, n, which is a dimensionless parameter combining the effects of electrical conductivity, applied magnetic field and the lubricant's couple stress behaviour. Therefore, the value of n directly affects the load carrying capacity of the contact.

$$n = \frac{2M}{a*} = \frac{2B_o h_o (\sigma/\mu)^{1/2}}{1/l*} = \frac{2B_o h_o (\sigma/\mu)^{1/2}}{1/\frac{l}{h_o}}$$

which simplifies to: $n = \frac{2M}{a*} = 2B_o l \sqrt{\frac{\sigma}{\mu}}$

It can be seen that for an assumed viscosity, n becomes a direct function of the magnetic field intensity, fluid electrical conductivity and the material constant η. By increasing these quantities, an enhancement in the value of n would be expected. This would yield better load carrying capacity. Analytical solution for three cases: case 1: $n<1$, case 2: $n=1$ and case3: $n>1$ are outlined in Appendix 3. Load carrying capacity is obtained by integration of pressure distribution p^* (derived in Appendix 3). Therefore, the dimensionless load carrying capacity (Note: $W=2\pi\int_b^a prdr$) for cases 1-3 becomes:

Case1: $\left(\frac{2M}{a*}\langle 1\right)$

$$W* = \frac{W h_o^3}{\mu a^4 V} = \frac{\pi}{2} \frac{\left(1+\gamma G*(M,a*,h*)\right)}{F*(M,a*,h*)} f(\lambda) \tag{18}$$

where:

$$f(\lambda) = \frac{(1-\lambda^4)}{4} + \frac{(\lambda^2-1)}{2} + \frac{(1-\lambda^2)}{\ln\lambda}\left(\frac{(\lambda^2-1)}{4} - \frac{\lambda^2}{2}\ln\lambda\right) \tag{19}$$

Case2: $\left(\frac{2M}{a*} = 1\right)$

$$W* = \frac{\pi}{2} \frac{\left(1+\gamma K*(M,a*,h*)\right)}{H*(M,a*,h*)} f(\lambda) \tag{20}$$

Case3: $\left(\frac{2M}{a*}\rangle 1\right)$

$$W* = \frac{\pi}{2} \frac{\left(1+\gamma Q*(M,a*,h*)\right)}{R*(M,a*,h*)} f(\lambda) \tag{21}$$

For a fixed load, the approach time to achieve a given gap needs to be calculated. The non-dimensional approach time and the non-dimensional centrifugal force-to-applied load ratio are:

$$t* = \frac{W h^2{}_o}{\mu a^4} t \qquad , \quad L = \frac{\rho a^4 \Omega^2}{W} \tag{22}$$

The time history of film thickness is obtained by making use of equations (18) ,(20) and (21) for cases 1, 2 and 3, respectively as:

Case1: $\left(\dfrac{2M}{a*} \langle 1 \right)$

$$\frac{dh*}{dt*} = \frac{1}{\pi f(\lambda)} \left(-2F*(M,a*,h*) + L\pi f(\lambda) G*(M,a*,h*) \right) \tag{23}$$

Case 2: $\left(\dfrac{2M}{a*} = 1 \right)$

$$\frac{dh*}{dt*} = \frac{1}{\pi f(\lambda)} \left(-2H*(M,a*,h*) + L\pi f(\lambda) K*(M,a*,h*) \right) \tag{24}$$

Case3: $\left(\dfrac{2M}{a*} \rangle 1 \right)$

$$\frac{dh*}{dt*} = \frac{1}{\pi f(\lambda)} \left(-2R*(M,a*,h*) + L\pi f(\lambda) Q*(M,a*,h*) \right) \tag{25}$$

The above equations are highly non-linear ordinary differential equations. Therefore, the solution method should shift from analytical to a numerical one. In order to achieve accurate results, a fourth-order Runge-Kutta method is used as well as the following initial conditions:

$h* = 1 \qquad$ at $\qquad t* = 0$

2.2- Application of MHD coupled stress to viscous coupling systems

An application of the current study is in the area of all-wheel drive (AWD) off-road vehicular differentials as highlighted by Sharaf et al [4], subject to manoeuvre on various soils [24]. In the traditional all-wheel drive systems, a viscous coupling is commonly installed on the propeller shaft in order to transmit the torque whilst allowing some difference in rotational speeds between the axles. These viscous coupling units are primarily used in off-road vehicles, but the methodology highlighted in this case study can easily be applied to other similar applications.

The viscous coupling unit consists of one set of inner plates which are splined onto a driving shaft and another set of outer plates, which are in turn splined onto the outer drum and then rigidly connected to the driven shaft. (figures 2 and3). The plates are separated by a thin film of silicone-based lubricant or electrically conducting coupled stress fluid in the presence of an external magnetic fluid. The main mechanism for torque transfer is based on the shearing of this thin fluid film. Therefore, the generated resistive torque of the viscous coupling is dependent on the relative speed of the rotating contacting elements, the plates' dimensions and the rheology of the fluid used.
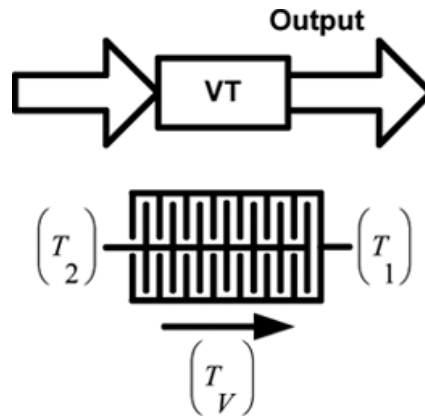
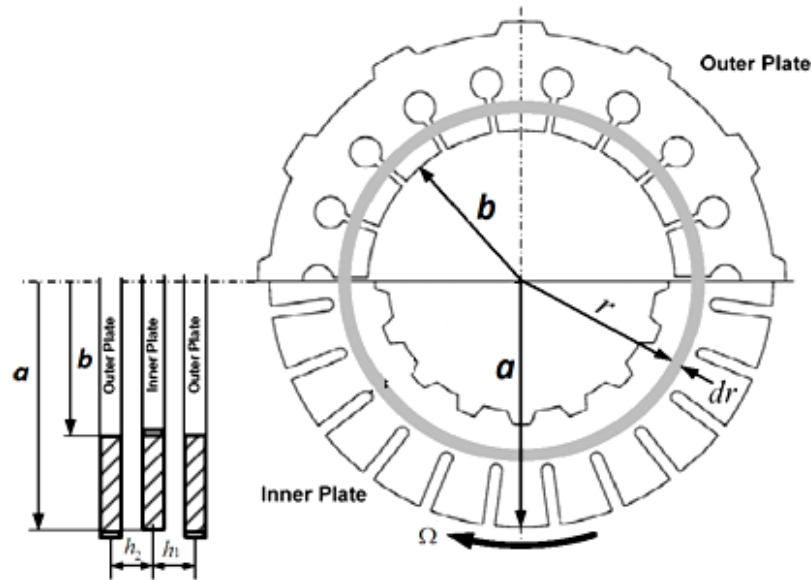Fig2. Simple schematic view of a viscous coupling

Fig3. Viscous shear mode configuration

In the present study, the effect of three types of lubricant used in this viscous coupling configuration are investigated. Other viscous couplers to mitigate powertrain torsional vibration or activation of engine cooling fan can also be considered. The lubricant types are: Type 1: A Newtonian lubricant, Type 2: A non – Newtonian silicone lubricant and Type3: An electrically conducting coupled stress lubricant in the presence of a magnetic field.

Type 1: Coupling through a Newtonian lubricant:

The total viscous shear torque T_v is given as [4]:

$$T_V = \frac{\pi \mu \Omega (a^4 - b^4)}{2 h_o} \tag{26}$$

Type 2: A non – Newtonian silicone-based lubricant:

The total viscous shear torque T_v is given as [4]:

$$T_V = \frac{2\pi \mu_s \Omega}{(\dot{\gamma} B)^m (4+m)} \left(\frac{\Omega}{h_o}\right)^{(1+m)} \left(a^{4+m} - b^{4+m}\right) \tag{27}$$

where m is the slope of viscosity-shear strain curve for the silicone-based lubricant.

Type 3: A coupled stress electrically conducting fluid:

Assuming an electrically conducting coupled stress fluid and isothermal conditions, the total viscous shear torque Tv, contributed by one side of the inner plate can be derived from basic principles by integrating the moment due to the shear stress over the active contact area from the inner plate radius b to the outer plate radius a as:

$$T_V = 2\pi \int_b^a \mu \frac{\partial v}{\partial z}\Big|_{z=h} r^2 dr \tag{28}$$

The generated torque depends on the value of $n = \dfrac{2M}{a*}$. Thus:

For Case1: $\left(\dfrac{2M}{a*} \langle 1\right)$

$$T_V = \frac{\pi \mu \Omega (a^4 - b^4)}{2 h_o (\beta^2 - \alpha^2)} \left[\beta^2 \alpha \coth\left(\frac{\alpha h}{h_o}\right) - \alpha^2 \beta \coth\left(\frac{\beta h}{h_o}\right)\right] \tag{29}$$

If $M=0$, $a^* \to \infty$ (i.e. $l^*=0$) and $h=h_o$. Thus, the above equation reduces to equation (26) which is the one derived by Sharaf et al [4] for a Newtonian fluid approximation of the silicone-based lubricant.

For Case 2: $\left(\dfrac{2M}{a*} = 1\right)$

$$T_V = \frac{\pi \mu \Omega (a^4 - b^4)}{2 h_o} \left[\frac{a*}{2\sqrt{2}} \coth\left(\frac{a*h}{\sqrt{2}\, h_o} \right) + \frac{h\, a*^2}{4 h_o \sinh^2\left(\frac{a*h}{\sqrt{2}\, h_o} \right)} \right] \tag{30}$$

and:

For Case3: $\left(\frac{2M}{a*} \rangle 1 \right)$

$$T_V = \frac{\pi \mu \Omega (a^4 - b^4)}{2 h_o\, (\beta_1^{\,2} - \alpha_1^{\,2})} \left[\beta_1^{\,2} \alpha_1 \coth\left(\frac{\alpha_1 h}{h_o} \right) - \alpha_1^{\,2} \beta_1 \coth\left(\frac{\beta_1 h}{h_o} \right) \right] \tag{31}$$

3- Results and discussion

The case of an electrically conducting coupled stress lubricant, intervening in the conjunction of a pair of parallel annular discs, subjected to a magnetic field is considered here. Tables 1-3 in Appendix 4 list the lubricant rheological, magnetic field and visco- lock system parameters used in the current study. In tables 1 and 2, the parameter, $a*$ represents the effect of coupled stresses, M provides the effect of externally applied magnetic field and the rotational inertial parameter, γ, defines the effect of lubricant inertia. It should be noted that only in the case 1:$(2M/a* < 1)$, l^* and M can diminish, which yields Newtonian and non-conducting fluids respectively. In cases 2 and 3: $M=0$ or $l^* = 0$ ($a* \to \infty$) would have no physical meaning and thus such cases cannot be interpreted.

As already noted, the MHD couple stress flow equation (analogous to Reynolds equation) in the presence of a magnetic field is derived using couple stress equations of motion, continuity of flow condition and rotational inertia. The important governing parameters are: (a)- the rotational parameter (shear strain rate), γ, which takes into account the effect of the rotational speed on the behaviour of a squeezing lubricant film, (b)- the dimensionless radius ratio, λ, (c)- the Hartmann number, M, denoting the effect of an externally applied magnetic field, and (d)- l^*, which signifies the effect of couple stress lubricant on the squeeze film performance. Based on these definitions, the flow characteristics of various squeezing film motion cases can be expected from a combination of these governing parameters. These combinations may be viewed as:

1.$M=0$, $l^* = 0$ ($a* \to \infty$), $\gamma=0$, $\lambda=0$: representing non-conducting Newtonian lubricants in pure squeeze between a pair of circular discs, a case studied by Hamrock [25] and Moore[26]. Assumption of Newtonian lubricant behaviour is, in general, idealised.
2. $M=0$, $l^* = 0$ ($a* \to \infty$), $\gamma \neq 0$, $\lambda \neq 0$: representing non-conducting Newtonian lubricants, under combined squeeze and shear as studied by Allen and McKillop [27].
3. $M \neq 0$, $l^* = 0$ ($a* \to \infty$), $\gamma=0$, $\lambda=0$: representing conducting Newtonian lubricants in the presence of a magnetic field in pure squeeze, reported by Kuzma [28] and Shukla [29]. This case represents active suspension elements for vehicles under relatively larger displacement.

4. $M{\neq}0$, $l^* = 0$ ($a^* {\rightarrow}{\infty}$), $\gamma{\neq}0$, $\lambda{=}0$: representing conducting Newtonian lubricants in the presence of a magnetic field, subjected to combined shear and squeeze, reported by Hsu et al [9].

5. $M{=}0$, $l^* {\neq} 0$, $\gamma{\neq}0$, $\lambda{=}0$: representing non-conducting couple stress lubricants in shear between a pair of rotating circular disc, studied by Lin et al [30]. Many torsional viscous dampers or couplers (such as in vehicular engine cooling fans) are examples of these conditions.

6. $M{\neq}0$, $l^* {\neq} 0$, $\gamma{\neq}0$, $\lambda{\neq}0$: representing conducting couple stress lubricants in the presence of a magnetic field, between rotating annular discs in shear and squeeze condition), studied here. There is a growing interest in such cases as active torque distribution devices in multi-axle vehicles or for off-road applications where driven wheels may experience varying contact patch conditions simultaneously, whilst on unmade terrains.

3.1- Case 1: $\frac{2M}{a^*} < 1$):

Figures 4-10 show the squeeze film characteristics for case 1. The pressure distribution for different values of M, $l^*$and γ are shown in figures 4-5. When the values of M and l^* increase (i.e. a stronger magnetic field, a decreasing value of a^*), the maximum lubricant pressure is naturally increased. On the other hand, when the rate of shear γ is increased, the maximum lubricant pressure is reduced. This is because a higher shear rate would constitute a thinner film. Therefore, if the film thickness is kept constant (as in figure 5) reduced pressures are expected to sustain a constant film at a greater rate of shear.
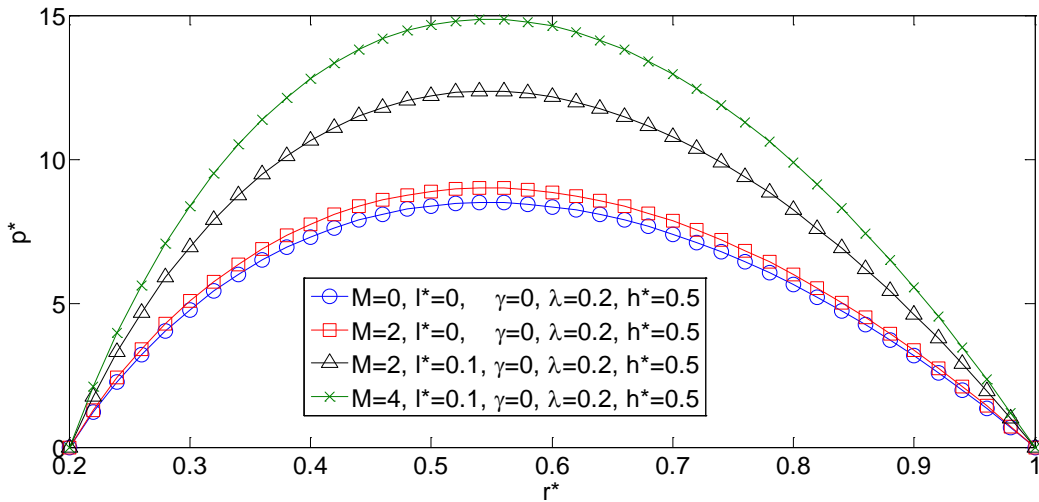

Fig.4. Variation of film pressure p^* with coordinate r^* in non- inertial case with $h^*{=}0.5$, $\lambda{=}0.2$

and different values of M, l^* for case 1: ($\frac{2M}{a^*} < 1$)
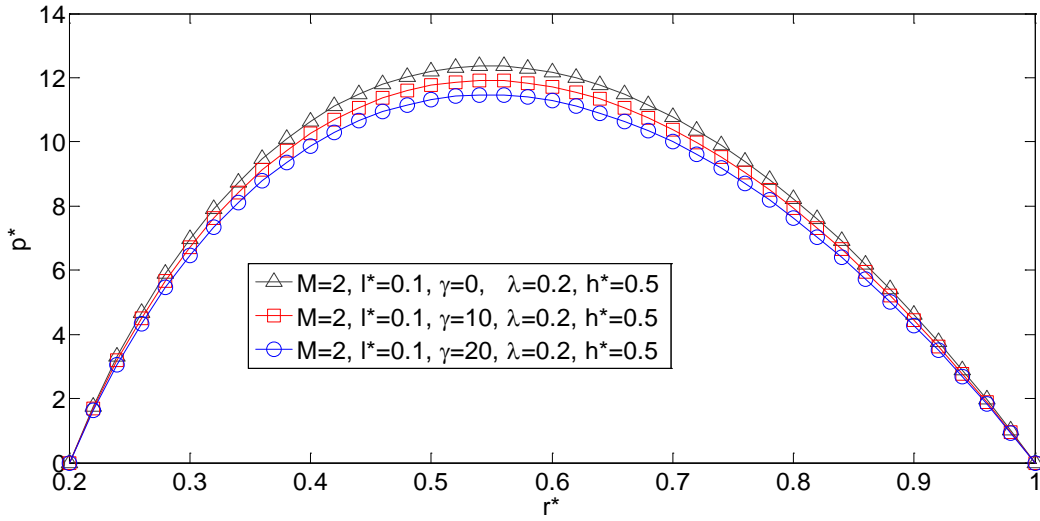
Fig.5. Variation of film pressure p^* with coordinate r^* at M=2, l^*=0.1 , h*=0.5 , λ=0.2

and different values of γ for case 1: $(\frac{2M}{a^*} < 1)$

Figures 6-8 show the variation of dimensionless load carrying capacity W^* with the coupled stress parameter l^*, Hartman number M and the radius ratio parameter λ at the dimensionless film thickness h^*=0.5. Since the coupled stress and MHD effects yield a higher film pressure, then the integrated load carrying capacity increases accordingly. In fact, as shown in Figures 6-8, the load carrying capacity is a function of l^* and M as would rationally be expected. This finding points to the least load carrying capacity for Newtonian, non - conducting fluids. By increasing the radius ratio parameter λ, the load carrying capacity is decreased. On the other hand, since the inertial parameter (shear rate) γ yields a lower film pressure, then the integrated load carrying capacity also decreases accordingly.
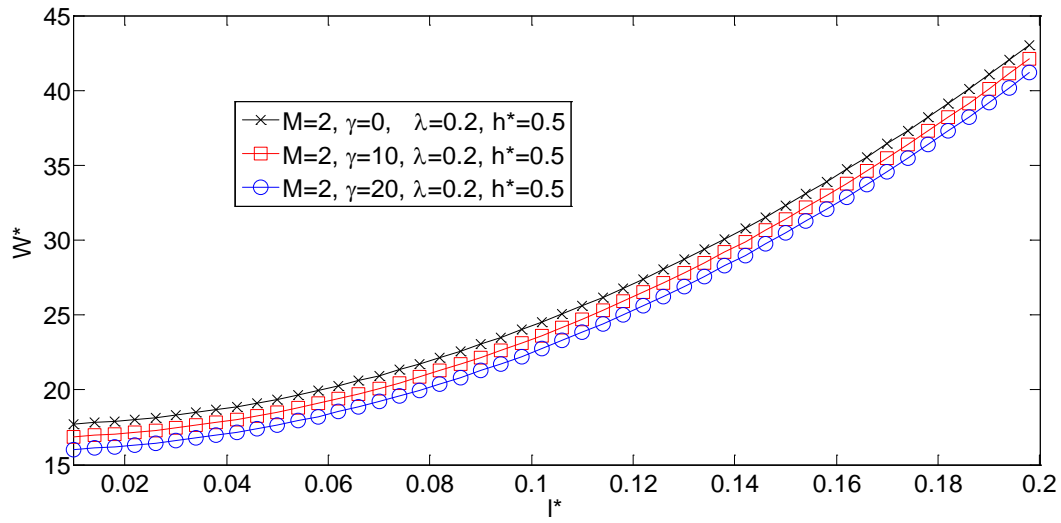
Fig.6. Variation of load-carrying capacity W^* with couple stress parameter l^* at h*=0.5,

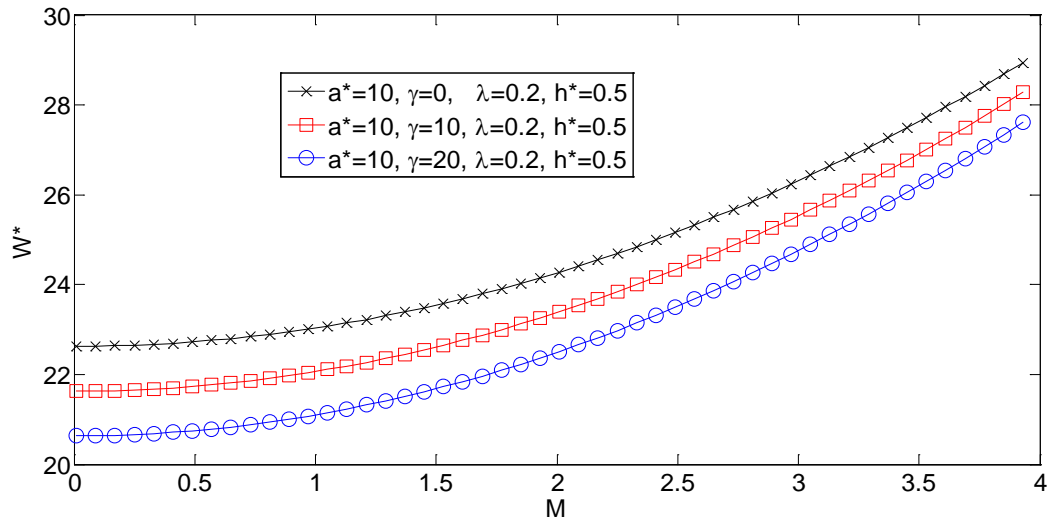M=2, λ=0.2and different values of γ for case 1: $(\frac{2M}{a^*} < 1)$

Fig.7. Variation of load-carrying capacity W^* with Hartman number M at h^*=0.5,

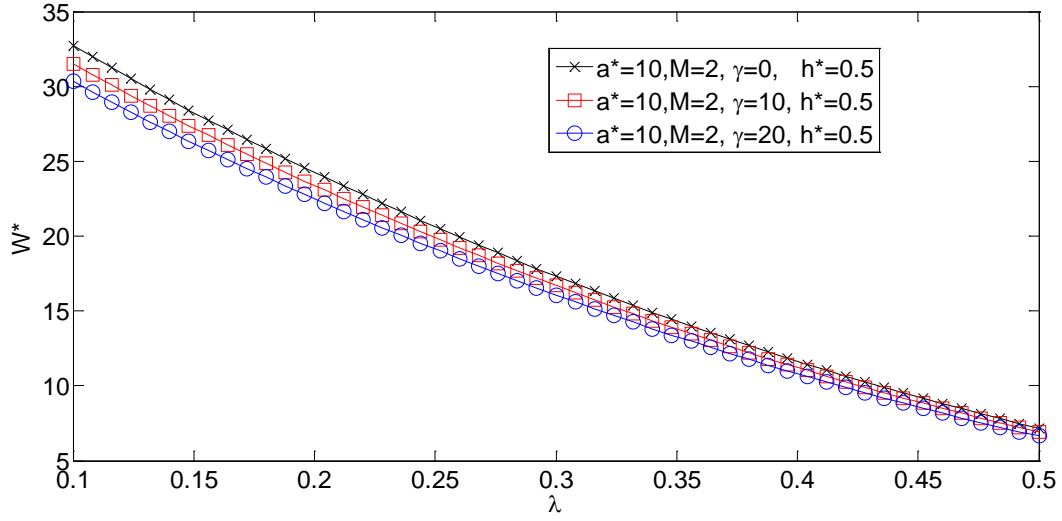l^*=0.1, λ=0.2 and different values of γ for case 1: $(\frac{2M}{a^*} < 1)$

Fig.8. Variation of the load-carrying capacity W^* with radius ratio parameter λ for different values of γ for case 1: $(\frac{2M}{a^*} < 1)$

Aside from load carrying capacity as a key performance measure meeting, operational functionality, and in order to guard against incidence of direct contact of solid surfaces, the response time to applied loads, particularly those leading to squeeze of the lubricant film is also an important measure of performance. The response time of the lubricant in a visco-lock system is crucial in distribution of torque in off-road vehicles on soft terrains under uneven contact patch conditions. Such circumstances may occur with a driving wheel induced-rutting in soft soil, with another wheel slipping at a higher speed [24].

Figures 9 and 10 show the variation of dimensionless film thickness h^* with dimensionless response time t^* for different values of the coupled stress parameter l^*, Hartman number M and rotational inertial parameter L. It is shown that for a coupled stress fluid ($l^*=0.1$) the response time is longer than for a Newtonian lubricant ($l^*=0$). Also, increasing the Hartman number M, leads to an increased response time. Figure 10 shows that the centrifugal force effect ($L = 10$) arising from the upper rotating disc decreases the response time to the squeezing motion as compared with the non-rotating case ($L = 0$). This is as the result of reduced build-up of pressure due to increased shear (also previously noted as an effect of increasing γ). Finally, smaller radius ratios result in longer response times, because of lower generated pressures over a larger effective contact area.

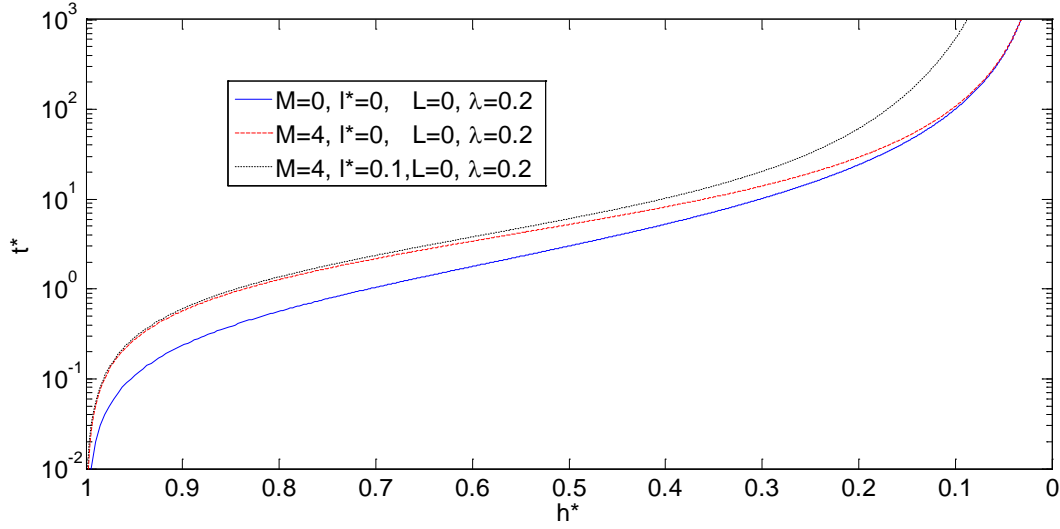Fig.9.Variation of film thickness h^* with response time t^* different values of M for case1: $(\frac{2M}{a^*} < 1)$
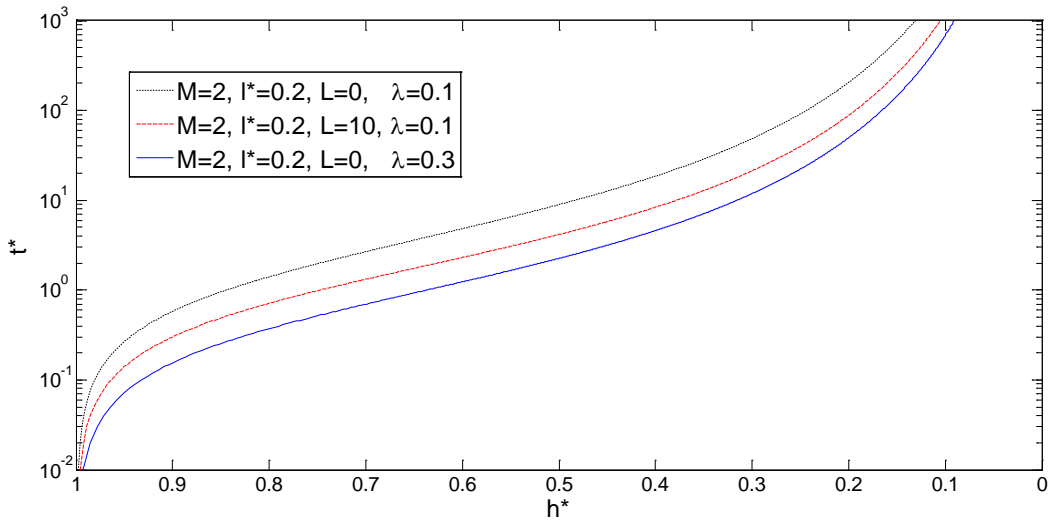

Fig.10.Variation of film thickness h^* with response time t^* for different values of L and λ for case1: $(\frac{2M}{a^*} < 1)$

For visco-lock devices tractive capacity (generated torque) is a key performance parameter. Figures 11 and 12 show the variation of the total viscous shear torque T with angular velocity Ω for different values of the Hartman number M and l^* with a constant dimensionless film thickness $h^*=0.5$. The geometrical parameters of discs are: a=10cm and b=8cm, and the viscosity of the lubricant is: 2.27×10^{-4} *Pa.s* with an initial assumed film thickness of: h_o= 0.25 *mm*. It can be observed from figures 11 and 12 that increasing the angular velocity Ω and the Hartman number M yield a greater driving torque, because the former increases the shear stress, thus friction, whilst the latter increases the load carrying capacity. The net effect in both cases is

15

increased traction, thus the driving torque.   Increasing the coupled stress parameter l^* also decreases the total viscous shear torque T (figure 12).

The variation of viscous shear torque T with Ω is shown in figure 13 for three different types of lubricant. These are: Type 1: A Newtonian approximation for a silicone-based fluid, Type2: a non- Newtonian approximation of a silicone-based fluid and Type3: an MHD coupled stress lubricant. Figure 13 shows that the MHD coupled stress lubricant generates a lower tractive action (viscous shear torque) than the silicone-based fluids. This is because the viscosity of silicone lubricant is higher than MHD coupled stress lubricant. However, there are two advantages in the use of the MHD coupled stress lubricant over the silicone-based fluids. Firstly, with slipping driven wheels or low torque requirements, lower viscosities promote higher efficiency (reduced frictional losses). Secondly, there is greater extent of control on generated torque by simply altering the Hartman number, M.   There is, however, the disadvantage of response time, as shown above and the additional instrumentation which would add to the vehicle weight.
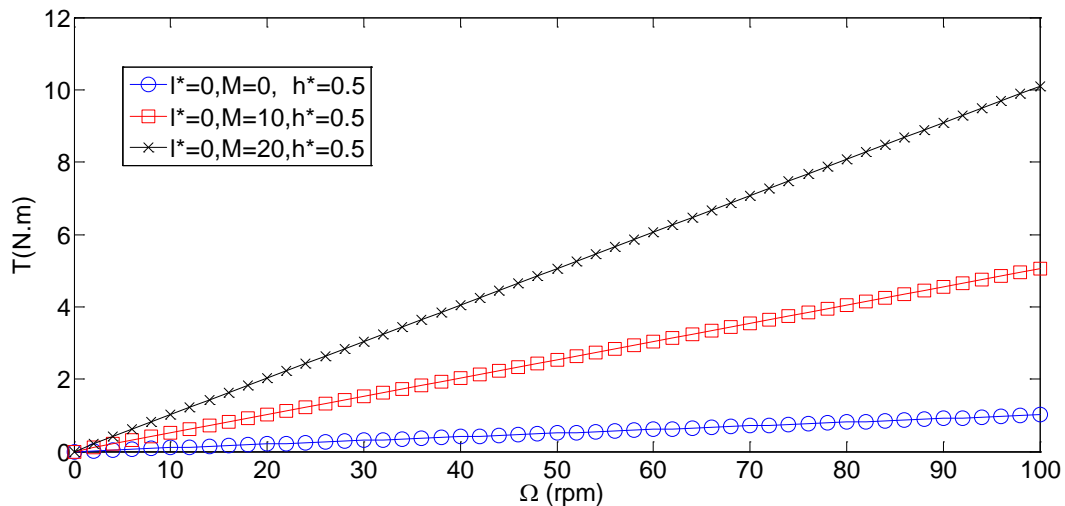

Fig.11.Variation of driving torque with differential rotational speed Ω at $h^* = 0.5$ and $l^*=0$ for different values of M for $a=0.1m$, $b=0.08m$,$\mu=0.000227$ $Pa.s$ and $h_o =0.00025m$. case 1: $(\frac{2M}{a^*} < 1)$
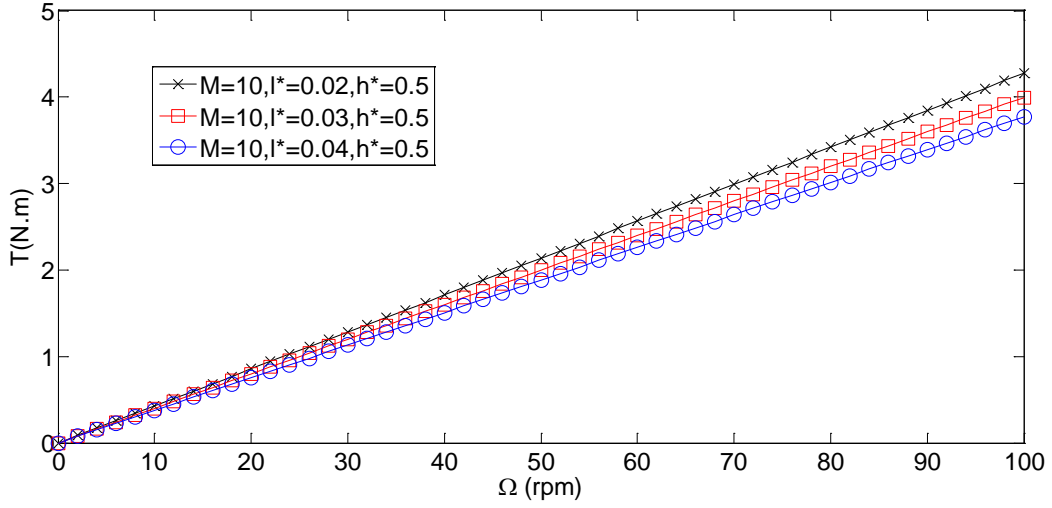
Fig.12. Variation of driving torque with differential rotational speed Ω at $h^* = 0.5$ and $M=10$ for different values of l^* for $a=0.1m$, $b=0.08m$, $\mu=0.000227$ $Pa.s$ and $h_o =0.00025m$. case 1: $(\frac{2M}{a^*} < 1)$
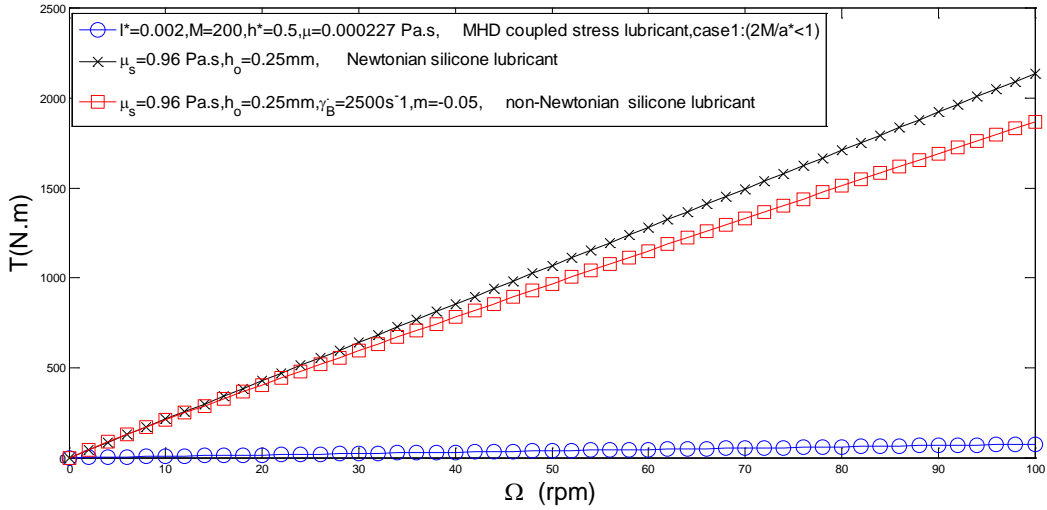

Fig.13. Variation of driving torque with differential rotational speed Ω for three types of lubricant: for $a=0.1m$, $b=0.8m$.

3.2- Case 2: $(\frac{2M}{a^*} = 1)$:

When case 2 is investigated, it is necessary to select values for M and a^* which satisfy the equality: $(\frac{2M}{a^*} = 1)$. Figure 14 shows the generated dimensionless pressure distribution p^* for different values of γ with $h^*= 0.5$ and $\lambda =10$. It is noted that an increasing shear rate γ results in decreasing p^* (a point previously noted). Figure 15 shows the variation of dimensionless load carrying capacity with rotational inertial parameter (shear rate) γ, for different values of λ. It is observed that by increasing γ and λ, load carrying capacity W^* is decreased, as previously

17

mentioned for case 1. Figure 16 shows the variation of film thickness h^* with the response time t^* for different values of L and λ. It is clear that with an increasing centrifugal force (inertial effect, increasing L) and the radius ratio parameter λ, the response time is reduced. In effect, there is a more effective tractive coupling with inertial effect over a larger effective contact domain. Figures 17 shows the variation of driving torque T with Ω for different values of M and a^* at h^*=0.5. It shows an increasing Hartman number M, inverse couple stress parameter a^* and Ω, all enhance the tractive action as would be expected.
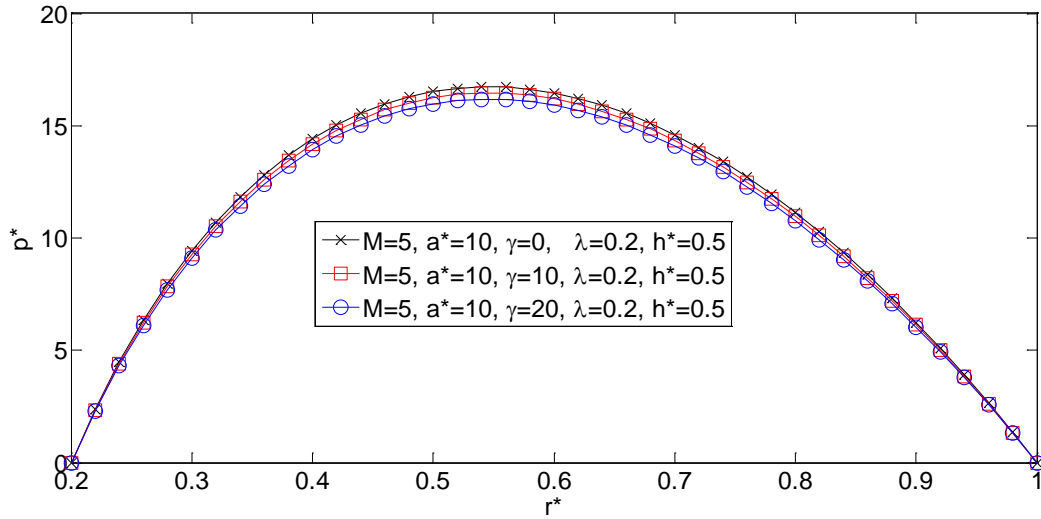

Fig.14. Variation of film pressure p^* with coordinate r^* at h^*=0.5, λ=0.2

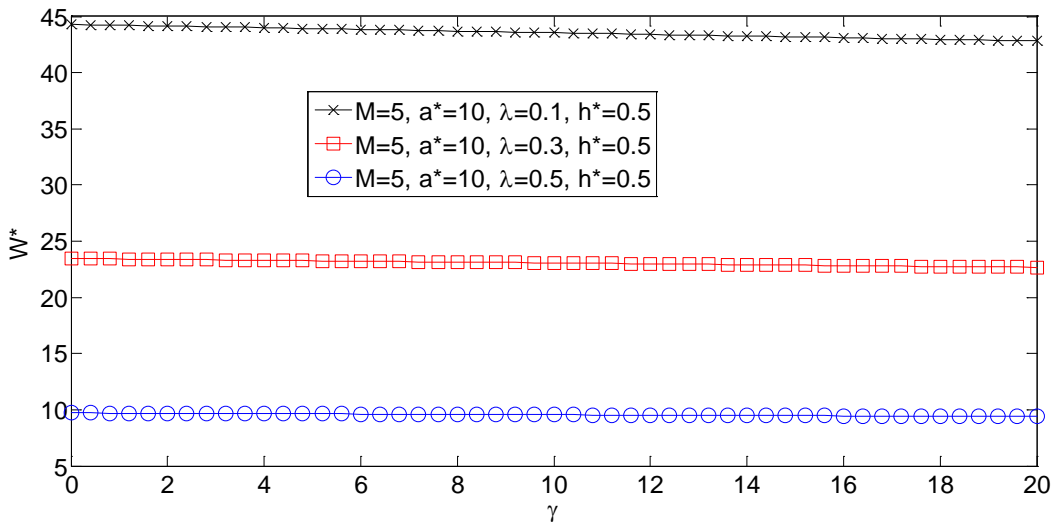and different values of γ for case 2: $(\frac{2M}{a^*} = 1)$

Fig.15. Variation of the load-carrying capacity W^* with rotational parameter γ at h^*=0.5 and different values of λ for case 2: $(\frac{2M}{a^*} = 1)$
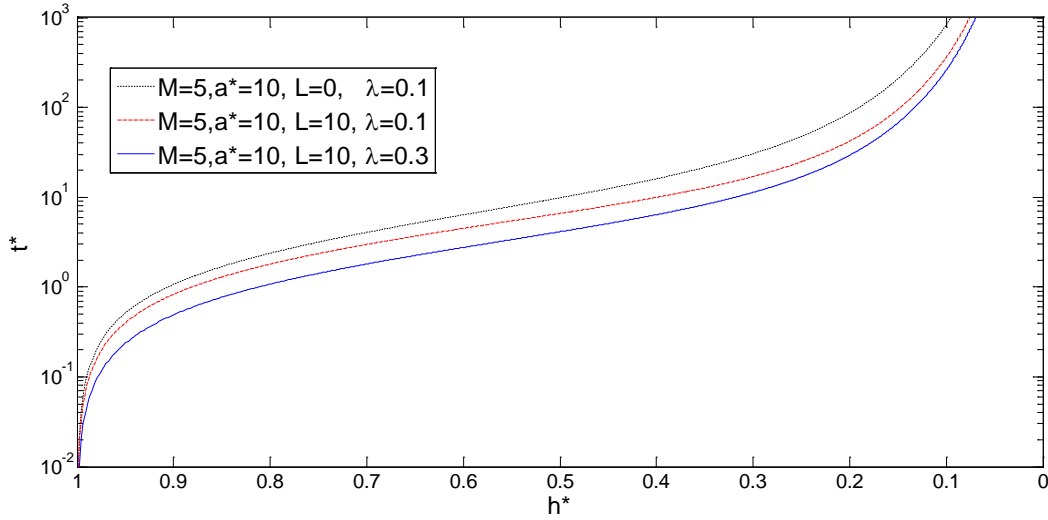
Fig.16. Variation of film thickness h^* with the response time t^* for different values of L, λ for case2: ($\frac{2M}{a^*} = 1$)
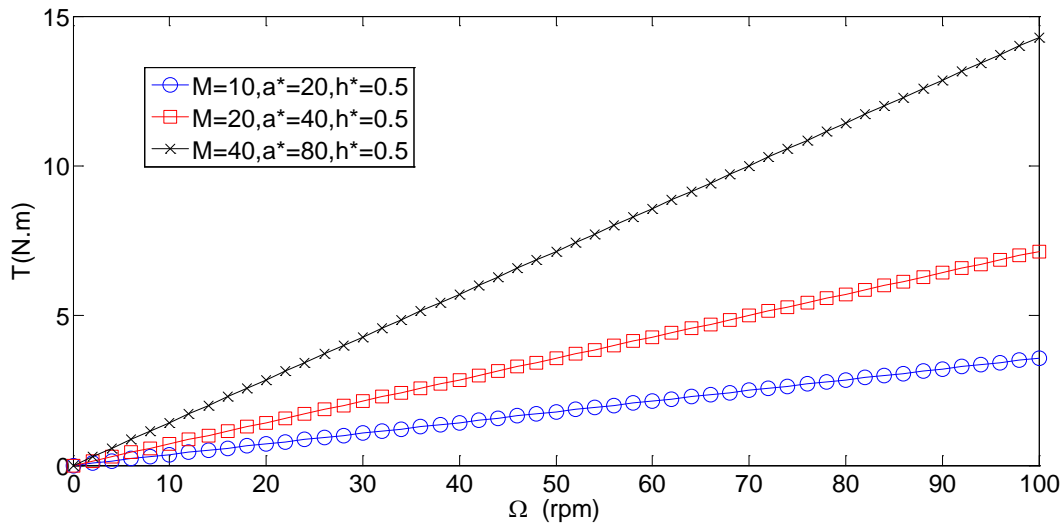

Fig.17. Variation of driving torque with Ω at h^*=0.5 and different values of M and a^* for case 2: ($\frac{2M}{a^*} = 1$)

3.3- Case 3: $\frac{2M}{a*} > 1$):

Figures 18- 21 show the squeeze film characteristics for case 3. For this case, the selected values for M and a^* should satisfy the above inequality. Dimensionless pressure distribution p^* is shown in Figure 18 for different values of rotational inertial parameter γ with $h^* = 0.5$, λ=0.2. With an increasing γ, the generated pressures and, thus, the load carrying capacity are decreased.

Figure.19 shows the variation of load capacity W^* with the couple stress parameter l^* for different values of γ under electrically conducting case; M=6. The choice of M=6 is because it satisfies the inequality $\frac{2M}{a*} > 1$ (case 3). As shown in figure 19, increasing the couple stress parameter l^* enhances the load carrying capacity, however, at the same time an increasing γ reduces the same. Figure 20 presents variation of load carrying capacity with the Hartman number for different values of λ. As it can be seen, using an electrically conducting fluid, in the presence of a magnetic field, the load carrying capacity is enhanced.

Figure 21 shows the variation of film thickness h^* with the lubricant response time t^* for different values of h^*. Figure 21 shows that the centrifugal force effect ($L = 10$) arising from the upper rotating disc decreases the response time when compared with the lubricant under pure squeeze condition ($L = 0$). This is in line with the previous findings with decreasing load carrying capacity with an increasing shear rate.

Figures 22 shows the variation of driving torque T with Ω for different values of M and a^* at h^*=0.5. It shows an increasing Hartman number M, inverse couple stress parameter a^* and Ω, all enhance the tractive action as would be expected.
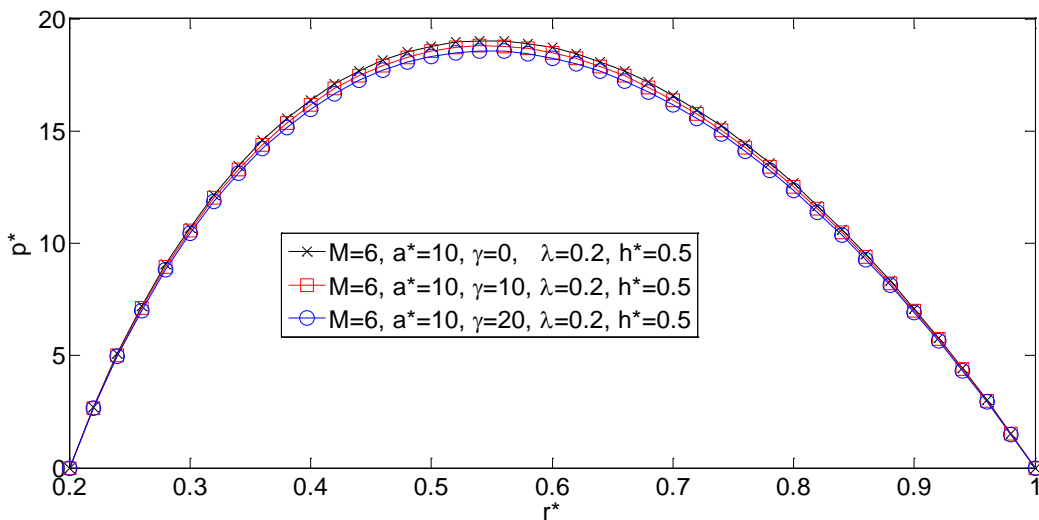

Fig.18. Variation of film pressure p^* with coordinate r^* with different values of γ at h^*=0.5 and

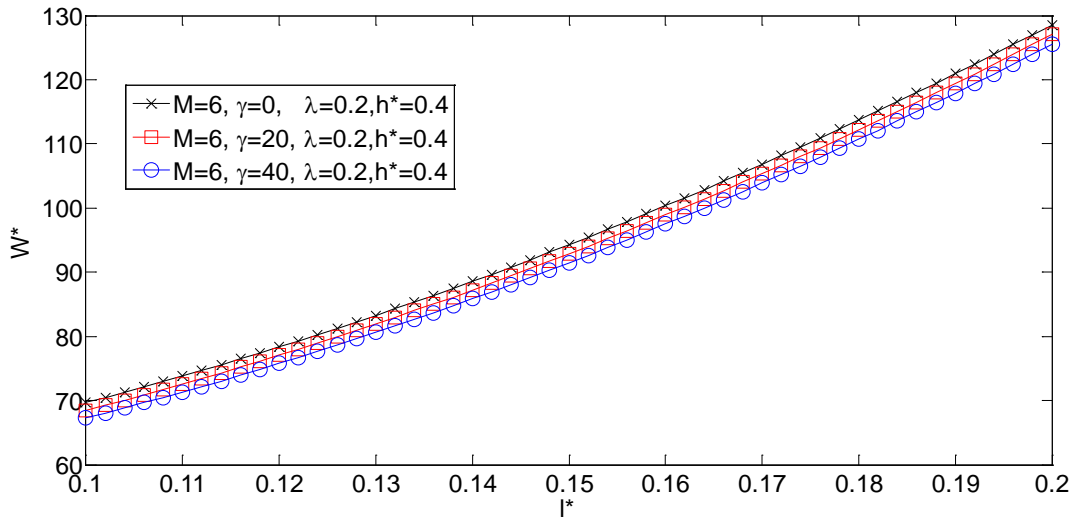λ=0.2 for case 3: ($\frac{2M}{a*} > 1$)

Fig.19. Variation of load-carrying capacity W^* with couple stress parameter l^* with h^*=0.4,

λ=0.2and different values of γ for case 3: $(\frac{2M}{a^*} > 1)$
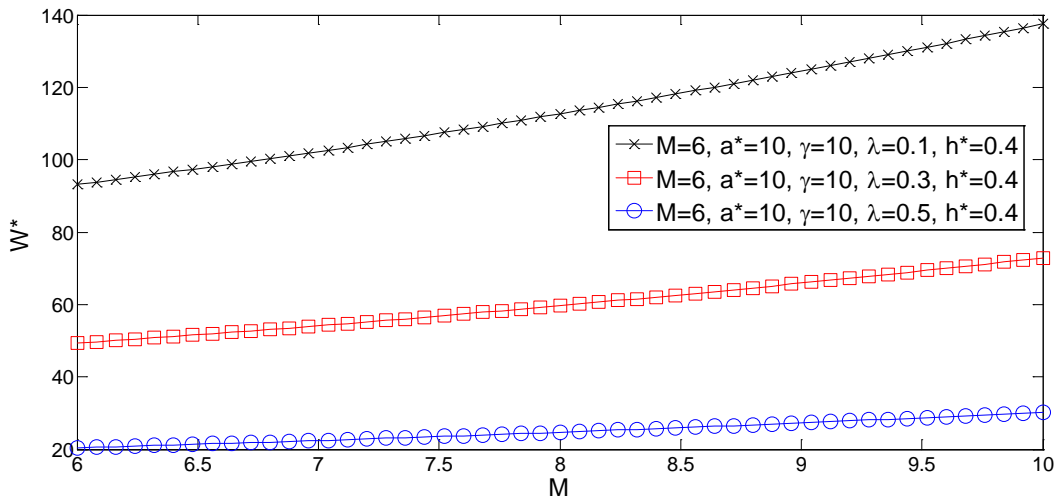
Fig.20. Variation of load carrying capacity W^* with the Hartman number with h^*=0.4 , γ=10

for different values of λ for case 3: $(\frac{2M}{a^*} > 1)$
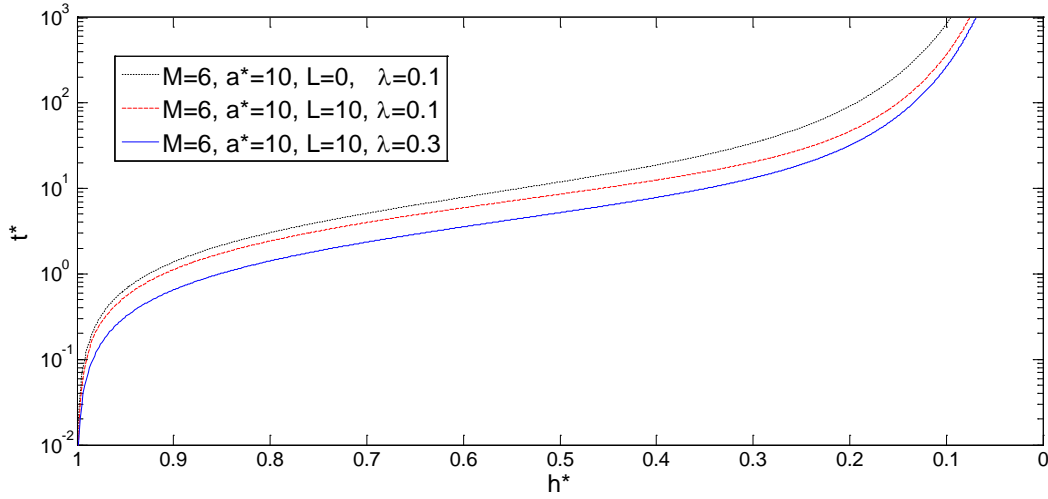
Fig.21.Variation of film thickness h^* with response time t^* for different values of L and λ for case3: $(\frac{2M}{a^*} > 1)$
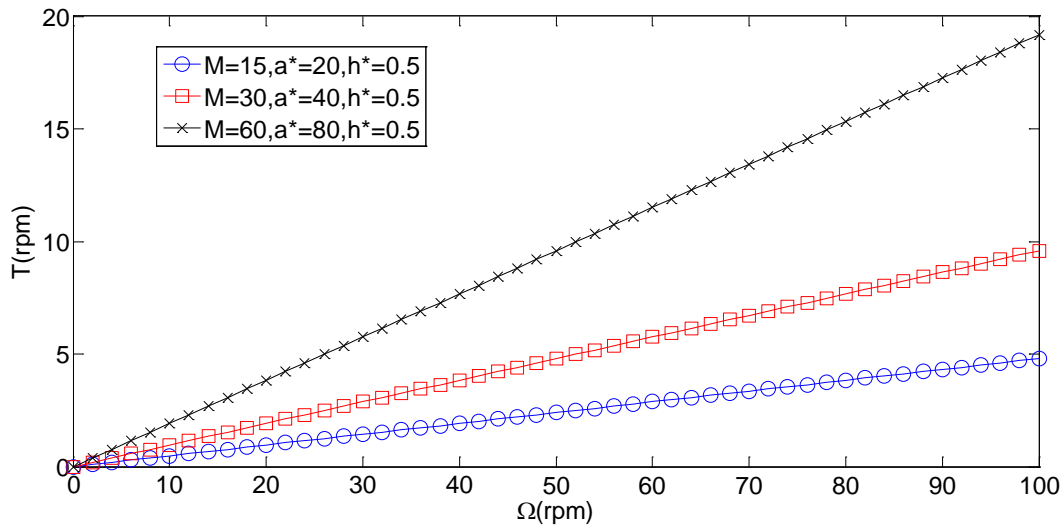
Fig.22.variation of driving torque with Ω at h^*=0.5 for different values of M and a^* for case 3: $(\frac{2M}{a^*} > 1)$

Figures 23 shows the variation of dimensionless load with λ for different value of n (n=0.4, n=1 , n=1,2) which represent the three different cases studied. This shows that increasing n enhances the load carrying capacity of the contact as would be expected.

Fig.23.Variation of the load-carrying capacity W^* with radius ratio parameter λ for different values of *n* at γ=20 and h*=0.5

4- Closure

Viscous coupling devices are increasingly used as torque distribution systems in vehicular drive train systems, particularly for AWD vehicles. In off-road applications wheel induce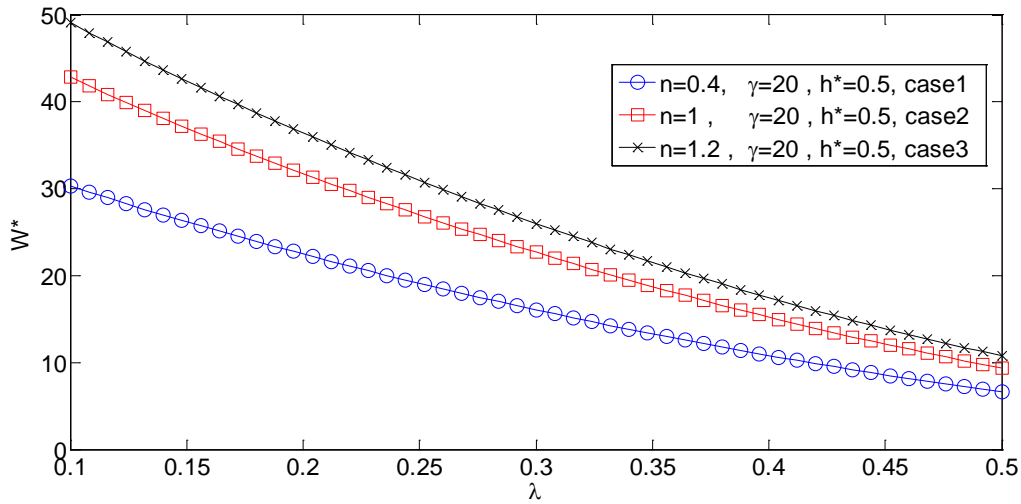d rutting on uneven and/or soft terrain it is essential to bias the driving torque to improve traction. Load carrying capacity, tractive efficiency and response times are essential design parameters. The paper undertakes a fundamental in-depth analysis of viscous coupling devices using various lubricant characteristics in squeeze and shear. They include the routinely analysed ideal Newtonian lubricants, non-Newtonian silicone-based fluids and couple stress fluids in the presence of a magnetic field. It is shown that better control of all key performance measures may be attained with couple stress fluids, although under the assumed isothermal condition the silicone-based fluids exhibit a faster response time. A more representative thermo-hydrodynamic analysis may alter this finding and represents the future direction of the current research.

Acknowledgment

References

[1] Mohammadpour, M., Theodossiades, S., Rahnejat, H. and Saunders, T. "Non-Newtonian mixed elastohydrodynamics of differential hypoid gears at high loads", Meccanica, 49, 2014, pp. 1115-1138, DOI 10.1007/s11012-013-9857-x

[2]- Barlow, T.J., Latham, S., McCrae, I.S. and Boulter, P.G., "A reference book of driving cycles for use in the measurement of road vehicle emissions", TRL Limited, version 3, 2009.

[3]- Mohammadpour, M., Rahmani, R. and Rahnejat, H. "Effect of cylinder deactivation on the tribo-dynamics and acoustic emission of overlay big end bearings", Proc. IMechE, J. Multi-body Dynamics, 228(2), 2014, pp. 138-151

[4]- Sharaf, A.M, Mavros, G., Rahnejat, H., King, P.D. and Mohan, S. K. "Optimisation of AWD off-road vehicle performance using visco-lock devices", Int. J. Heavy Vehicle Systems, 15, 2008, pp. 188- 207.

[5] Maki, E.R. and Kuzma, D.C. "Magneto hydrodynamic lubrication flow between parallel plates". J. Fluid Mech., 26 1966, pp. 534–43.

[6] Usha, R. and Vimala, P. "Magneto hydrodynamic squeeze film characteristics between parallel circular plates containing a single central air bubble in the inertial flow regime". J. Applied Mechanics, 66, 1999, pp. 1021–1023.

[7] Lin, J.R., Lu, R.F. and Liao, W.H. "Analysis of magneto-hydrodynamic squeeze film characteristics between curved annular plates", Ind. Lubrication and Tribology, 56, 2004, pp. 300–305.

[8] Lin, R.F. "Magneto-hydrodynamic squeeze film characteristics between annular discs". Ind. Lubrication and Tribology, 53, 2001, pp.66-71.

[9] Hsu, C.H., Lai, C., Hung, C.R. and Lin, J.R. "Magneto-hydrodynamic squeeze film characteristics between circular disks including rotational inertial effects", Proc. IMechE, Part J: J. Engineering Tribology, 222, 2007, pp.157–164

[10] Agrawal, V.K. "Inertia effects in hydro magnetic inclined slider bearing", Jap. J. Appl. Physics, 9, 1970, pp.820-824.

[11] Anwar, M..I. and Rodkiewicz, C.M. "Non-uniform magnetic field effects in MHD slider bearings", Trans. ASME, J. Lubn. Tech. 94, 1972, pp.101-105.

[12] Gupta, J.L. and Bhat, M.V. "An inclined porous slider bearing with a transverse magnetic field", Wear, 55, 1979, pp. 359–67.

[13].Eringen, A . C , "Simple micro- fluids", Int. J. Eng. Sci., 2, 1964, pp .205-217

[14]. Eringen, A . C , "microcontinuum field theories -1:Fluent media", Springer,New York,2001

[15]. Eringen, A . C, "Theory of micropolar fluid", J. Math. Mech.16, 1966, P. 1

[16] Ariman, T. and Sylvester, N.D. "Micro-continuum fluid mechanics, a review", Int. J. Eng. Sci., 11, 1973, pp. 905-930.

[17] Ariman T. and Sylvester, N.D. "Applications of micro continuum fluid mechanics",. Int. J. Eng. Sci., 12, 1974, pp. 273-293.

[18] Stokes, V.K. "Couple stresses in fluids", Phys. of Fluids, 9, 1966, pp.1709-1715.

[19]- Eringen, A.C., "Theory of micropolar elasticity", Springer, New York, 1999

[20]- Chen, J., Lee, J.D. and Liang, C., "Constitutive Equations of Micropolar Electromagnetic Fluids", J. Non-Newtonian Fluids, 166, 2011, pp. 867-874

[21] Ramanaish, G. and Sarkar, P. "Squeeze films and thrust bearings lubricated by fluids with couple stress", Wear, 48, 1978, pp. 309-16.

[22] Das, N.C. " A study of optimal load-bearing capacity for slider bearing lubricated with couple stress fluids in magnetic field", Trib. Int., 31, 1998, pp.393-400.

[23] Daliri M, Jalali-Vahid, D and Rahnejat, H. "Squeeze film lubrication of coupled stress electrically conducting inertial fluids in wide parallel rectangular conjunctions subjected to a magnetic field", Proc. IMechE, Part J: J. Eng. Tribology, 228(3), 2014, pp. 288-302, doi: 10.1177/1350650113504565

[24]- Sharaf, A.M., Rahnejat, H. and King, P.D. "Analysis of handling characteristics of all-wheel-drive off-road vehicles", Int. J. Heavy Vehicle Systems, 15, 2008, pp. 89-106

[25] Hamrock, B.J. "Fundamentals of fluid film lubrication", McGraw-Hill, New York, 1994

[26] Moore, D. F. "A review of squeeze films", Wear, 8, 1965, pp. 245–263.

[27] Allen, C. W. and McKillop, A. A. "An investigation of the squeeze film between rotating annuli", Trans. ASME, J. Lubn. Tech., 92, 1970, pp. 435–441.

[28] Kuzma, D. C. "Magneto hydrodynamic squeeze films", Trans ASME, J. Basic Eng., 86, 1964, pp. 441–444.

[29] Shukla, J. B. "Hydromagnetic theory for squeeze films", Trans ASME, J. Basic Eng., 90, 1965, pp. 142–144.

[30] Lin J.R and Hung C.R. "Combined effects of non-Newtonian rheology and rotational inertia on the squeeze film characteristics of parallel circular discs", Trans ASME, J. Engineering Tribology, 222, 2008, pp. 629-636

Appendix1: Nomenclature

a , b	Outer radius and the inner radius of the discs, respectively	B_o	applied magnetic field
l	characteristic length of the additives, $(\frac{\eta}{\mu})^{\frac{1}{2}}$	h_o	film thickness at t=0
M	Hartman number , $B_o \, h_o \sqrt{\frac{\sigma}{\mu}}$	r^*	coordinate, $r^* = \frac{r}{a}$ (dimensionless)
W^*	dimensionless load-carrying capacity, $\frac{Wh_o^3}{\mu a^4 V}$	V	squeezing velocity, $-\frac{dh}{dt}$
t , t^*	response time , $\frac{Wh_o^2}{\mu a^4} t$	p, p^*	squeeze film pressure, $\frac{ph_o^3}{\mu a^2 V}$
σ	electrical conductivity	μ	lubricant viscosity
γ	Rotational inertia, $\frac{\rho h_o^3 \Omega^2}{\mu V}$	η	material constant responsible for couple stress fluids
		ρ	lubricant density
u^*	dimensionless velocity in the r direction, $\frac{\mu u}{h_o^2(-g_p)}$	λ	ratio of inner radius to the outer radius, b/a
a^*	inverse couple stress parameter, $\frac{h_o}{l}$	l^*	couple stress parameter, $\frac{l}{h_o}$
g_p	pressure gradient	h, h^*	Film thickness, $\frac{h}{h_o}$ (dimensionless)
u , v, w	velocity component in the r , θ and z directions, respectively	L	non-dimensional centrifugal force-applied load ratio, $\frac{\rho a^4 \Omega^2}{W}$
		m	Slope of viscosity-shear

	strain curve for silicone lubricant
	$\dot{\gamma}, \dot{\gamma}_B$ Shear strain rate and critical shear strain rate for silicone
	μ_s viscosity of silicone
	Ω angular velocity of upper disc
	v^* dimensionless velocity in θ direction. $v/r\,\Omega$
	r , θ , z cylindrical coordinates
	z^* dimensionless coordinate. z/h_o
	T_V total viscous shear torque
	n dimensionless criteria parameter

Appendix 2:

The governing equations for predicting the behaviour of an incompressible couple stress, electrically conducting fluid in the presence of a magnetic field were initially introduced by Stokes [18] as:

$$\rho\left(\frac{\partial \vec{V}}{\partial t} + \vec{V}.\nabla \vec{V}\right) = -\nabla p + \mu \nabla^2 \vec{V} - \eta \frac{\partial^4 \vec{V}}{\partial z^4} + \vec{J} \times \vec{B} \tag{32}$$

In equation (5) the left hand term introduces the inertia forces and the right hand ∇p is the pressure gradient, $\mu \nabla^2 \vec{V}$ is viscous force, and $\eta \frac{\partial^4 \vec{V}}{\partial z^4}$ introduces the couple stress effect based on [18]. $\vec{J} \times \vec{B}$ is Lorentz force, where $\vec{J}$ and $\vec{B}$ are the current density and magnetic field vectors, respectively.

According to Shukla [29] for hydromagnetic lubrication one can use equations (33)-(40) as follows:

$$\nabla.\vec{V} = 0 \tag{33}$$

$$\nabla.\vec{B} = 0 \tag{34}$$

$$\nabla \times \vec{B} = \vec{J} \tag{35}$$

$$\nabla.\vec{E} = 0 \tag{36}$$

$$\nabla \times \vec{E} = 0 \tag{37}$$

$$\vec{J} = \sigma[\vec{E} + (\vec{V} \times \vec{B})] \tag{38}$$

where In the above equations, $\vec{E}$ is electric field vector and σ is electrical conductivity of the lubricant.

Now the following assumptions are made:

1. the intensity of applied magnetic field in the z direction is constant.

2. the induced magnetic fields in the directions of r and θ (B_r , B_θ) are neglected.

3. the induced electric fields $\vec{E}$ in all directions are ignored.

Applying the above conditions/assumptions, the components in equation (32) become:

$$-\rho\frac{v^2}{r} = -\frac{\partial p}{\partial r} + \mu\frac{\partial^2 u}{\partial z^2} - \eta\frac{\partial^4 u}{\partial z^4} + J_\theta B_z \tag{39}$$

$$0 = \mu\frac{\partial^2 v}{\partial z^2} - \eta\frac{\partial^4 v}{\partial z^4} - J_r B_z \tag{40}$$

$$\frac{\partial p}{\partial z} = 0 \tag{41}$$

By Neglecting the electrical field (assumption3), equation (38) can be written as:

$$\vec{J} = \sigma(\vec{V} \times \vec{B}) \tag{42}$$

By resolving $\vec{J}$ in the three directions; r, θ and z and carrying out the vector cross-product $(\vec{V} \times \vec{B})$ equation (m) becomes:

$$J_r e_r + J_\theta e_\theta + J_z e_z = \sigma[(vB_z - wB_\theta)e_r + \sigma(wB_r - uB_z)e_\theta + \sigma(uB_\theta - wB_r)e_z] \tag{43}$$

Then:

$$J_r = \sigma(vB_z - wB_\theta) \tag{44}$$

$$J_\theta = \sigma(wB_r - uB_z) \tag{45}$$

$$J_z = \sigma(uB_\theta - wB_r) \tag{46}$$

Now letting: $B_r = B_\theta = 0$ (assumption 2) and also $B_z = B_o$ (assumption 1), equations (43)-(46) can be written as:

$$J_r = \sigma vB_o \tag{47}$$

$$J_\theta = -\sigma uB_o \tag{48}$$

$$J_z = 0 \tag{49}$$

Substituting equations (47)-(49) into equations (39)-(41) yields the governing equation (1)-(3).

Appendix 3:

To obtain the contact load carrying capacity, it is necessary to determine the lubricant film pressure distribution, p^*. This, in turn, requires the evaluation of velocity distribution in the contact conjunction. Therefore:

For velocity component in the θ-direction:

Case 1 : $\dfrac{2M}{a*} \langle 1$

$$v* = \frac{1}{\beta^2 - \alpha^2}\left[\beta^2\left(\frac{\sinh \alpha z*}{\sinh \alpha h*}\right) - \alpha^2\left(\frac{\sinh \beta z*}{\sinh \beta h*}\right)\right] \tag{50}$$

Case 2 : $\dfrac{2M}{a*} = 1$

$$v* = \left(\dfrac{\dfrac{2a*}{\sqrt{2}}\sinh\left(\dfrac{a*h*}{\sqrt{2}}\right) + \dfrac{h*a*^2}{2}\cosh\left(\dfrac{a*h*}{\sqrt{2}}\right)}{\dfrac{2a*}{\sqrt{2}}\sinh^2\left(\dfrac{a*h*}{\sqrt{2}}\right)} \right)\sinh\left(\dfrac{a*z*}{\sqrt{2}}\right) - \dfrac{a*z*\cosh\left(\dfrac{a*z*}{\sqrt{2}}\right)}{2\sqrt{2}\sinh\left(\dfrac{a*h*}{\sqrt{2}}\right)} \qquad (51)$$

Case 3 : $\dfrac{2M}{a*}\rangle 1$

$$v* = \dfrac{1}{\beta_1^{\,2} - \alpha_1^{\,2}}\left[\beta_1^{\,2}\left(\dfrac{\sinh\alpha_1 z*}{\sinh\alpha_1 h*}\right) - \alpha_1^{\,2}\left(\dfrac{\sinh\beta_1 z*}{\sinh\beta_1 h*}\right) \right] \qquad (52)$$

For velocity component in the *r*-direction:

Case 1 : $n = \dfrac{2M}{a*}\langle 1$

$$u* = \dfrac{-1}{M^2}\left\{ -1 + \dfrac{1}{\alpha^2 - \beta^2}\left[\beta^2\left(\dfrac{\sinh\left(\alpha\left(z*-h*\right)\right) - \sinh\alpha z*}{\sinh\alpha h*}\right) - \alpha^2\left(\dfrac{\sinh\left(\beta(z*-h*)\right) - \sinh\beta z*}{\sinh\beta h*}\right) \right] \right\} (53)$$

Case 2 : $n = \dfrac{2M}{a*} = 1$

$$u* = \dfrac{-1}{M^2}\left(\begin{array}{l} -1 + \left[\dfrac{\left(-\cosh\left(\dfrac{a*h*}{\sqrt{2}}\right)+1\right)}{\sinh\left(\dfrac{a*h*}{\sqrt{2}}\right)} + \dfrac{\dfrac{\sqrt{2}\,a*h*}{4}\left(-\cosh\left(\dfrac{a*h*}{\sqrt{2}}\right)+1\right)\cosh\left(\dfrac{a*h*}{\sqrt{2}}\right)}{\sin^2 h\left(\dfrac{a*h*}{\sqrt{2}}\right)} + \dfrac{\sqrt{2}\,a*h*}{4} \right]\sinh\left(\dfrac{a*z*}{\sqrt{2}}\right) \\[4em] +\cosh\left(\dfrac{a*z*}{\sqrt{2}}\right) - \dfrac{\sqrt{2}\,a*z*}{4}\sinh\left(\dfrac{a*z*}{\sqrt{2}}\right) + \dfrac{\sqrt{2}a*z*}{4}\dfrac{\left(\cosh\left(\dfrac{a*h*}{\sqrt{2}}\right)-1\right)}{\sinh\left(\dfrac{a*h*}{\sqrt{2}}\right)}\cosh\left(\dfrac{a*z*}{\sqrt{2}}\right) \end{array} \right) (54)$$

Case 3 : $n = \dfrac{2M}{a*}\rangle 1$

$$u* = \frac{-1}{M^2}\left\{-1 + \frac{1}{\alpha_1^2 - \beta_1^2}\left[\beta_1^2\left(\frac{\sinh(\alpha_1(z*-h*)) - \sinh\alpha_1 z*}{\sinh\alpha_1 h*}\right) - \alpha_1^2\left(\frac{\sinh(\beta_1(z*-h*)) - \sinh\beta_1 z*}{\sinh\beta_1 h*}\right)\right]\right\} \quad (55)$$

where $\alpha = \frac{a*}{\sqrt{2}}\left(1 + \sqrt{1 - \frac{4M^2}{a*^2}}\right)^{\frac{1}{2}}$, $\beta = \frac{a*}{\sqrt{2}}\left(1 - \sqrt{1 - \frac{4M^2}{a*^2}}\right)^{\frac{1}{2}}$ and

$$\alpha_1 = \frac{a*}{\sqrt{2}}\left(1 + i\left(\sqrt{\frac{4M^2}{a*^2} - 1}\right)\right)^{\frac{1}{2}} \quad , \quad \beta_1 = \frac{a*}{\sqrt{2}}\left(1 - i\left(\sqrt{\frac{4M^2}{a*^2} - 1}\right)\right)^{\frac{1}{2}}$$

Now, let $u = \frac{-h_o^2(g_p)}{\mu}u*$ and substitute into the continuity of flow equation (4) and integrate with respect to z over the film thickness. Then, substituting for u^* from the above equations and Making use of non-dimensional parameters as follow:

$$r* = \frac{r}{a} \quad , \quad p* = \frac{ph_o^3}{\mu a^2 V}, \gamma = \frac{\rho h_o^3 \Omega^2}{\mu V} \quad (56)$$

The non- dimensional Reynolds equations is derived for different three cases as follow

$$\text{Case1}\left(n = \frac{2M}{a*}\langle 1\right)$$

$$\frac{1}{r*}\frac{\partial}{\partial r*}(r*\frac{\partial p*}{\partial r*}) = \frac{(1 + \gamma G*(M,a*,h*))}{F*(M,a*,h*)} \quad (57)$$

where:

$$F*(M,a*,h*) = \frac{1}{M^2} \times$$

$$\left\{-h* + \frac{1}{\alpha^2 - \beta^2}\left(\frac{\beta^2}{\sinh(\alpha h*)}\left(\frac{2}{\alpha} - \frac{2}{\alpha}\cosh(\alpha h*)\right) - \frac{\alpha^2}{\sinh(\beta h*)}\left(\frac{2}{\beta} - \frac{2}{\beta}\cosh(\beta h*)\right)\right)\right\} \quad (58)$$

and:

$$G^*(M,a^*,h^*) = \frac{-1}{M^2(\alpha^2-\beta^2)^3} \times$$

$$\left\{ \frac{16\alpha^3\beta^4\sinh^2(\frac{\alpha h^*}{2})\left(1-2\sinh^2(\frac{\beta h^*}{2})\right)+\alpha^5\beta^2\sinh^2(\beta h^*)\left(4+12\sinh^2(\frac{\alpha h^*}{2})\right)}{(\alpha^2-4\beta^2)\sinh(\alpha h^*)\sinh^2(\beta h^*)} + \right.$$

$$\frac{16\alpha^4\beta^3\sinh^2(\frac{\beta h^*}{2})\left(1-2\sinh^2(\frac{\alpha h^*}{2})\right)+\alpha^2\beta^5\sinh^2(\alpha h^*)\left(4+12\sinh^2(\frac{\beta h^*}{2})\right)}{(4\alpha^2-\beta^2)\sinh(\beta h^*)\sinh^2(\alpha h^*)} +$$

$$\frac{4\beta^6\cosh^2(\frac{\alpha h^*}{2})\sinh^2(\alpha h^*)-16\beta^6\sinh^2(\frac{\alpha h^*}{2})}{3\alpha\sinh^3(\alpha h^*)}+\frac{16\alpha^6\sinh^2(\frac{\beta h^*}{2})-4\alpha^6\sinh^2(\beta h^*)\cosh^2(\frac{\beta h^*}{2})}{3\beta\sinh^3(\beta h^*)}+$$

$$\left. \frac{-\alpha^3\beta^4\left(8+24\sinh^2(\frac{\alpha h^*}{2})\right)}{(4\alpha^2-\beta^2)\sinh(\alpha h^*)}+\frac{-\alpha^4\beta^3\left(8+24\sinh^2(\frac{\beta h^*}{2})\right)}{(\alpha^2-4\beta^2)\sinh(\beta h^*)} \right\}$$

$$-\frac{1}{M^2(\alpha^2-\beta^2)^2}\times\left\{ h^*(\alpha^4+\beta^4)+\frac{(\alpha^2\beta^4-\beta^6-4\alpha^4\beta^2)\coth(\alpha h^*)}{\alpha(\alpha^2-\beta^2)} + \right.$$

$$\left. \frac{(\alpha^6-\alpha^4\beta^2+4\alpha^2\beta^4)\coth(\beta h^*)}{\beta(\alpha^2-\beta^2)}-h^*\left(\beta^4\coth^2(\alpha h^*)+\alpha^4\coth^2(\beta h^*)\right) \right\} \tag{59}$$

case 2: $\left(\dfrac{2M}{a*}=1\right)$

$$\frac{1}{r*}\frac{\partial}{\partial r*}(r*\frac{\partial p*}{\partial r*})=\frac{\left(1+\gamma\,K*(M,a*,h*)\right)}{H*(M,a*,h*)}\tag{60}$$

where:

$$H*(M,a*,h*)=\frac{1}{M^{2}}\left\{-h*-\frac{\dfrac{a*h*}{2}-\dfrac{3\sqrt{2}\sinh(\dfrac{a*h*}{\sqrt{2}})}{2}}{a*\cosh^{2}(\dfrac{\sqrt{2}\,a*h*}{4})}\right\}\tag{61}$$

and

$$K*(M,a*,h*)=\frac{2}{M^{2}\left(6912\,a*\left(\cosh(\dfrac{\sqrt{2}\,a*h*}{2})-1\right)^{2}\left(\cosh(\dfrac{\sqrt{2}\,a*h*}{2})+1\right)^{3}\right)}\times$$

$$\left\{\begin{array}{l}700\sqrt{2}\sinh(\sqrt{2}\,a*h*)-1056\,a*h*-350\sqrt{2}\sinh(2\sqrt{2}\,a*h*)+1510\sqrt{2}\sinh(\dfrac{\sqrt{2}\,a*h*}{2})-\\[2ex]325\sqrt{2}\sinh(\dfrac{3\sqrt{2}\,a*h*}{2})-107\sqrt{2}\sinh(\dfrac{5\sqrt{2}\,a*h*}{2})+720\,a*^{3}\,h*^{3}+616\,a*h*\cosh(\sqrt{2}\,a*h*)+\\[2ex]440\,a*h*\cosh(2\sqrt{2}\,a*h*)+2748\,a*h*\cosh(\dfrac{\sqrt{2}\,a*h*}{2})-2748\,a*h*\cosh(\dfrac{3\sqrt{2}\,a*h*}{2})+\\[2ex]288\,a*^{3}\,h*^{3}\cosh(\sqrt{2}\,a*h*)+360\,a*^{3}\,h*^{3}\cosh(\dfrac{\sqrt{2}\,a*h*}{2})+72\,a*^{3}\,h*^{3}\cosh(\dfrac{3\sqrt{2}\,a*h*}{2})+\\[2ex]2208\sqrt{2}\,a*^{2}\,h*^{2}\sinh(\sqrt{2}\,a*h*)-408\sqrt{2}\,a*^{2}\,h*^{2}\sinh(\dfrac{\sqrt{2}\,a*h*}{2})+264\sqrt{2}\,a*^{2}\,h*^{2}\sinh(\dfrac{3\sqrt{2}\,a*h*}{2})\end{array}\right\}\tag{62}$$

case 3: $\left(\dfrac{2M}{a*}\rangle 1\right)$

$$\frac{1}{r*}\frac{\partial}{\partial r*}(r*\frac{\partial p*}{\partial r*}) = \frac{\left(1+\gamma Q*(M,a*,h*)\right)}{R*(M,a*,h*)} \tag{63}$$

where

$$R*(M,a*,h*) = \frac{1}{M^2} \times$$

$$\left\{-h*+\frac{1}{\alpha_1{}^2-\beta_1{}^2}\left(\frac{\beta_1{}^2}{\sinh(\alpha_1 h*)}\left(\frac{2}{\alpha_1}-\frac{2}{\alpha_1}\cosh(\alpha h*)\right)-\frac{\alpha_1{}^2}{\sinh(\beta_1 h*)}\left(\frac{2}{\beta_1}-\frac{2}{\beta_1}\cosh(\beta_1 h*)\right)\right)\right\} \tag{64}$$

and

$$Q^*(M,a^*,h^*) = \frac{-1}{M^2(\alpha_1{}^2 - \beta_1{}^2)^3} \times$$

$$\left\{ \begin{array}{l}
\dfrac{16\alpha_1{}^3\beta_1{}^4 \sinh^2(\dfrac{\alpha_1 h^*}{2})\left(1 - 2\sinh^2(\dfrac{\beta_1 h^*}{2})\right) + \alpha_1{}^5\beta_1{}^2 \sinh^2(\beta_1 h^*)\left(4 + 12\sinh^2(\dfrac{\alpha_1 h^*}{2})\right)}{(\alpha_1{}^2 - 4\beta_1{}^2)\sinh(\alpha_1 h^*)\sinh^2(\beta_1 h^*)} + \\[4mm]
\dfrac{16\alpha_1{}^4\beta_1{}^3 \sinh^2(\dfrac{\beta_1 h^*}{2})\left(1 - 2\sinh^2(\dfrac{\alpha_1 h^*}{2})\right) + \alpha_1{}^2\beta_1{}^5 \sinh^2(\alpha_1 h^*)\left(4 + 12\sinh^2(\dfrac{\beta_1 h^*}{2})\right)}{(4\alpha_1{}^2 - \beta_1{}^2)\sinh(\beta_1 h^*)\sinh^2(\alpha_1 h^*)} + \\[4mm]
\dfrac{4\beta_1{}^6 \cosh^2(\dfrac{\alpha_1 h^*}{2})\sinh^2(\alpha_1 h^*) - 16\beta_1{}^6 \sinh^2(\dfrac{\alpha_1 h^*}{2})}{3\alpha_1 \sinh^3(\alpha_1 h^*)} + \dfrac{16\alpha_1{}^6 \sinh^2(\dfrac{\beta_1 h^*}{2}) - 4\alpha_1{}^6 \sinh^2(\beta_1 h^*)\cosh^2(\dfrac{\beta_1 h^*}{2})}{3\beta_1 \sinh^3(\beta_1 h^*)} + \\[4mm]
\dfrac{-\alpha_1{}^3\beta_1{}^4\left(8 + 24\sinh^2(\dfrac{\alpha_1 h^*}{2})\right)}{(4\alpha_1{}^2 - \beta_1{}^2)\sinh(\alpha_1 h^*)} + \dfrac{-\alpha_1{}^4\beta_1{}^3\left(8 + 24\sinh^2(\dfrac{\beta_1 h^*}{2})\right)}{(\alpha_1{}^2 - 4\beta_1{}^2)\sinh(\beta_1 h^*)} +
\end{array} \right\}$$

$$-\frac{1}{M^2(\alpha_1{}^2 - \beta_1{}^2)^2} \times$$

$$\left\{ \begin{array}{l}
h^*(\alpha_1{}^4 + \beta_1{}^4) + \dfrac{(\alpha_1{}^2\beta_1{}^4 - \beta_1{}^6 - 4\alpha_1{}^4\beta_1{}^2)\coth(\alpha_1 h^*)}{\alpha_1(\alpha_1{}^2 - \beta_1{}^2)} \\[4mm]
\dfrac{(\alpha_1{}^6 - \alpha_1{}^4\beta_1{}^2 + 4\alpha_1{}^2\beta_1{}^4)\coth(\beta_1 h^*)}{\beta_1(\alpha_1{}^2 - \beta_1{}^2)} - h^*\left(\beta_1{}^4 \coth^2(\alpha_1 h^*) + \alpha_1{}^4 \coth^2(\beta_1 h^*)\right)
\end{array} \right\} \qquad (65)$$

the non – dimensional form of boundary conditions (9) , (10) are :

$$p^* = 0 \text{ at } r^* = \lambda \qquad (66)$$

$$p^* = 0 \text{ at } r^* = 1 \qquad (67)$$

where

$$\lambda = \frac{b}{a}$$

(68)

is the ratio of the inner radius to the outer radius

Integrating pressure gradient $(\frac{\partial p*}{\partial r*})$ with respect to r^{*} and applying boundary conditions (66), (67), the MHD couple stress squeeze film pressure in film region is obtained for three cases respectively as follow

Expressed in a non-dimensional form, it yields:

Case1 $\left(\frac{2M}{a*} \langle 1 \right)$

$$p* = \frac{\left(1 + \gamma\, G*(M,a*,h*)\right)}{4F*(M,a*,h*)}\left(r*^{2} - 1 + \frac{(1-\lambda^{2})}{\ln\lambda}\ln r* \right)$$

(69)

$\lambda \leq r* \leq 1$

Case 2: $\left(\frac{2M}{a*} = 1 \right)$

$$p* = \frac{\left(1 + \gamma\, K*(M,a*,h*)\right)}{4H*(M,a*,h*)}\left(r*^{2} - 1 + \frac{(1-\lambda^{2})}{\ln\lambda}\ln r* \right)$$

(70)

$\lambda \leq r* \leq 1$

Case3: $\left(\frac{2M}{a*} \rangle 1 \right)$

$$p* = \frac{\left(1 + \gamma\, Q*(M,a*,h*)\right)}{4R*(M,a*,h*)}\left(r*^{2} - 1 + \frac{(1-\lambda^{2})}{\ln\lambda}\ln r* \right)$$

(71)

$\lambda \leq r* \leq 1$

Appendix 4:

Table 1: Lubricant rheology

parameter name	symbol	Value	Unit
initial film thickness	h_o	4×10^{-5}	(metre) m
outer radius of disc	a	0.2	(metre) m
inner radius of disc	b	0.04	(metre) m
rotational speed	Ω	1985.18	(radians per second) $rads/s$
lubricant viscosity	μ	2.27×10^{-4}	(Pascal-second) $Pa.s$
couple stress material constants	η	0.3632×10^{-14}	(Newton-second) $N.s$
lubricant density	ρ	900	Kg/m^3
squeezing velocity	V	0.1	m/s
characteristic length of the additives	l	4×10^{-6}	(metre) m
Ratio of inner radius to the outer radius	λ	0.2	-
couple stress parameter	l^*	0.1	-
inverse couple stress parameter	a^*	10	-
rotational inertia parameter	γ	10	-

Table 2: Parameters of the magnetic field

Parameter name	Symbol	Value	Unit
Initial film thickness	h_o	4×10^{-5}	(metre) m
Lubricant viscosity	μ	2.27×10^{-4}	(Pascal-second) $Pa.s$
Electrical conductivity	σ	2.216×10^5	(Siemens per meter) S/m
Magnetic field	Bo	4	(Weber per square metre) wb/m^2
Hartman number	M	5	-

Table 3: Visco-lock system Parameters

Parameter name	Symbol	Value	Unit
Initial film thickness	h_o	2.5×10^{-4}	(metre) m
Differential speed range between inner and outer plates	Ω	0-100	(revolution per minute) rpm
critical shear strain rate of silicone lubricant	$\dot{\gamma}_B$	2500	(s^{-1})
Silicone lubricant viscosity	μ_s	0.96	(Pascal-second) Pa.s
Slope of viscosity-shear strain curve for silicone lubricant	m	-0.05	-
Silicone lubricant density	ρ	960	(kilograms per cubic metre)kg/m^3
Outer plate radius	a	0.1	(metre) m
inner plate radius	b	0.8	(metre) m